Global and Planetary Change 172 (2019) 140–149

Contents lists available at ScienceDirect

Global and Planetary Change

journal homepage: www.elsevier.com/locate/gloplacha

The role of abrupt climate change in the formation of an open vegetation enclave in northern Amazonia during the late Quaternary

André Zular[a,*], André Oliveira Sawakuchi[a], Cristiano Mazur Chiessi[b], Fernando Mendonça d'Horta[c], Francisco William Cruz[a], José Alexandre Melo Demattê[d], Camila Cherem Ribas[e], Gelvam André Hartmann[f], Paulo César Fonseca Giannini[a], Emílio Alberto Amaral Soares[g]

[a] Instituto de Geociências, Universidade de São Paulo, Rua do Lago 562, São Paulo, 05508-080, Brazil
[b] Escola de Artes, Ciências e Humanidades, Universidade de São Paulo, São Paulo, Brazil
[c] Programa de Pós-Graduação em Genética, Conservação e Biologia Evolutiva, Instituto Nacional de Pesquisas da Amazônia, Manaus, Brazil
[d] Departmento de Ciências do Solo, Colégio de Agricultura Luiz de Queiroz, Universidade de São Paulo, Piracicaba, Brazil
[e] Coordenação de Biodiversidade, Instituto Nacional de Pesquisas da Amazônia, Manaus, Brazil
[f] Instituto de Geociências, Universidade Estadual de Campinas, Campinas, Brazil
[g] Departamento de Geociências, Universidade Federal do Amazonas, Manaus, Brazil

ARTICLE INFO

Keywords:
Amazon forest
Climate change
Heinrich Stadial 1
Last Glacial Maximum
Open vegetation
White sand vegetation

ABSTRACT

The effects of climate changes on biotic expansion or divergence is a widely debated topic. This discussion is particularly relevant for northern Amazonia where patches of open vegetation environments that harbor high endemic and specialized species are present in a matrix of tall closed canopy forest. This paper presents the depositional chronology and evolution of an 8.7-m thick stabilized fluvial and eolian sediment profile in a sandy plain substrate that underpins the largest open vegetation enclave in northern Amazonia. Three depositional units were identified using optically stimulated luminescence and radiocarbon ages coupled with grain size, magnetic susceptibility, and reflectance analyses. A lower unit of coarse fluvial silt deposited between 53 and 28 ka is overlain unconformably by a 5-m thick middle unit of fine eolian sand deposited at high accumulation rates between the Last Glacial Maximum (23–19 ka) and Heinrich Stadial 1 (HS1; 18.1–14.7 ka) when persistent and long-lasting shifts of the Intertropical Convergence Zone (ITCZ) to the Southern Hemisphere promoted dry and windy conditions in northern South America. An upper ~2-m thick unit was deposited when the climate became wetter after HS1, promoting the formation of soils that support open vegetation habitats. This study indicates that abrupt millennial-scale climate events can induce significant changes in the Amazonian landscape, which in turn play an essential role in the distribution and diversification of specialized biota.

1. Introduction

The Branco River catchment (Negro River basin) in Brazil and Guyana encompasses several enclaves of open vegetation embedded within the Terra Firme (non-flooded) forests that dominate northern Amazonia (north of Negro River, Fig. 1; Anderson, 1981). Such open vegetation environments harbor distinct fauna and flora assemblages when compared to the surrounding upland forests and bear a high level of endemism (e.g., Anderson, 1981; Fine et al., 2010; Mittermeier et al., 2010; Borges et al., 2016; Fine and Baraloto, 2016; Matos et al., 2016;). Also, they are widely distributed in Amazonia, representing ~8% of its total area but are split into patches that vary between 1 km^2 and 40,000 km^2 (Adeney et al., 2016). The distribution of these patches is strongly correlated with substrate characteristics and pedogenic processes following the deposition of sands (Quesada et al., 2012; Honorio Coronado et al., 2015). For example, Amazonian sandy substrates formed by eolian (e.g., Carneiro Filho et al., 2002), or alluvial depositional systems (e.g., Rossetti et al., 2012; Rossetti, 2014; Cremon et al., 2016) host diverse vegetation types such as savanna (known regionally as cerrado or lavrado) and white sand vegetation (WSV; Adeney et al., 2016 and references therein). Savannas develop on soils where the water table is deeper and harbor vegetation types such as scrubs, herbs, detached patches of forests, and forests at the bank of rivers (e.g., Carvalho and Carvalho, 2012). In turn, WSV habitats are associated

* Corresponding author at: Instituto de Geociências, Universidade de São Paulo, Rua do Lago 562, 05508-080, São Paulo-SP, Brazil.
E-mail address: andrezular@usp.br (A. Zular).

https://doi.org/10.1016/j.gloplacha.2018.09.006
Received 7 June 2018; Received in revised form 2 September 2018; Accepted 6 September 2018
Available online 11 September 2018
0921-8181/ © 2018 Elsevier B.V. All rights reserved.

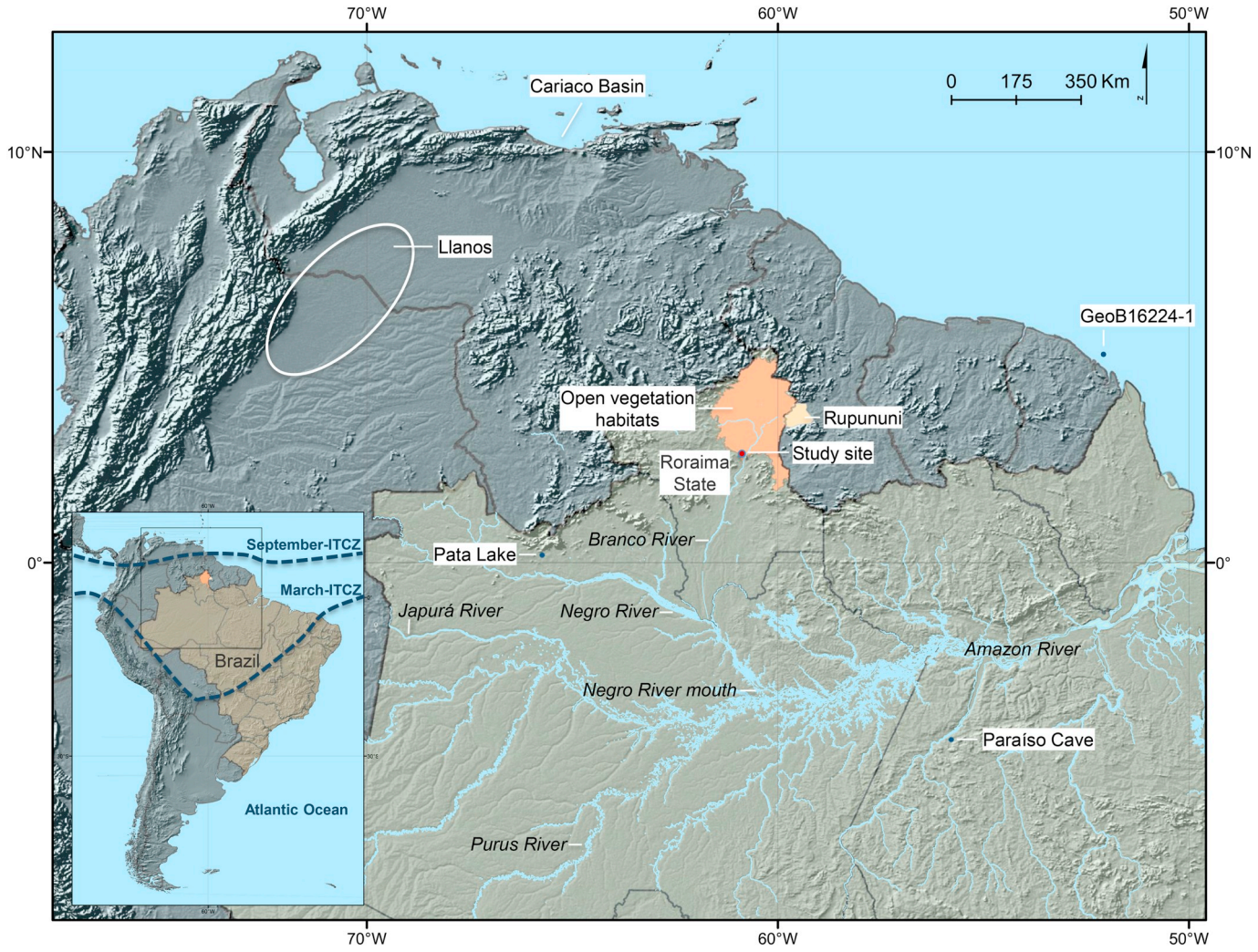

Fig. 1. Digital elevation model (SRTM) of northern South America showing the location of open vegetation habitats in Roraima State and Rapununi savanna. The Brazilian Amazon major river systems and sites mentioned in the text are also shown. Intertropical Convergence Zone northerly and southerly ranges shown in the inset are current mean positions.

with Entisols to Spodosols (Quesada et al., 2012; Mendonça et al., 2014), harboring from open grass-and shrublands to low-stature forests (known regionally as campina and campinarana, respectively; e.g., Adeney et al., 2016).

Various studies have attempted to explain how climate, tectonics, or a combination of both, have shaped these enclaves underlain by sandy substrates (e.g., Colinvaux, 1987; Rossetti, 2014; Cremon et al., 2016). However, there is no consensus on the chronology of the sand deposition, with estimates ranging from the late Pleistocene to the Holocene (e.g., Latrubesse and Nelson, 2001; Carneiro Filho et al., 2002). Contrastingly, other authors suggest that these substrates are much older, having been formed through the weathering of ancient rocks, though they provide no chronology of these events (Quesada et al., 2010). Furthermore, few paleoclimate studies focusing on the evolution of open vegetation habitats have been conducted in the Branco River catchment and the contiguous Rupununi sands (Fig. 1). Latrubesse and Nelson (2001) propose a detailed geologic and geomorphologic framework of these areas coupled with regional paleoclimate data. Their findings suggest a period of dune building during the Last Glacial Maximum (LGM); however, their research lacks direct chronological evidence. Teeuw and Rhodes (2004) conclude that the onset of eolian activity in the Rupununi savanna occurred between 17 and 15 ka (thousand years ago). These authors obtained optically stimulated luminescence (OSL) chronology in a 1.8 m pit where the bottommost sample calculated age was 15 ka. However, the 17 ka age was extrapolated considering a uniform rate of sediment accumulation. Recently, work on the sedimentary terraces of the Branco River revealed OSL ages up to 18.7 ka (Cremon et al., 2016).

This paper investigates the evolution of the most extensive open vegetation habitat in northern Amazonia through the reconstruction of paleoclimate conditions in the Branco River catchment. To accomplish this aim, we analyzed an 8.7-m thick profile of stabilized fluvial and eolian sediments in the upper Branco River. First, a detailed chronology was determined by OSL and radiocarbon dating. Subsequently, a heavy mineral analysis was performed to investigate the provenance of sediments. Finally, to identify periods of dune activity or stabilization, we obtained paleoclimate proxies based on grain size, magnetic susceptibility, and light reflectance. These proxies are sensitive to changes in precipitation, thus elucidating the evolution of northern Amazonian sandy substrates and their overlaying open vegetation responses to late Quaternary climate changes.

1.1. Study site

Remote sensing images and geomorphological features observed in the field (Fig. 2c and d, respectively) show that the study area is part of relatively well preserved, or in some sectors degraded, parabolic dunefield encompassing ~9 km^2. This dunefield is bounded on the W and

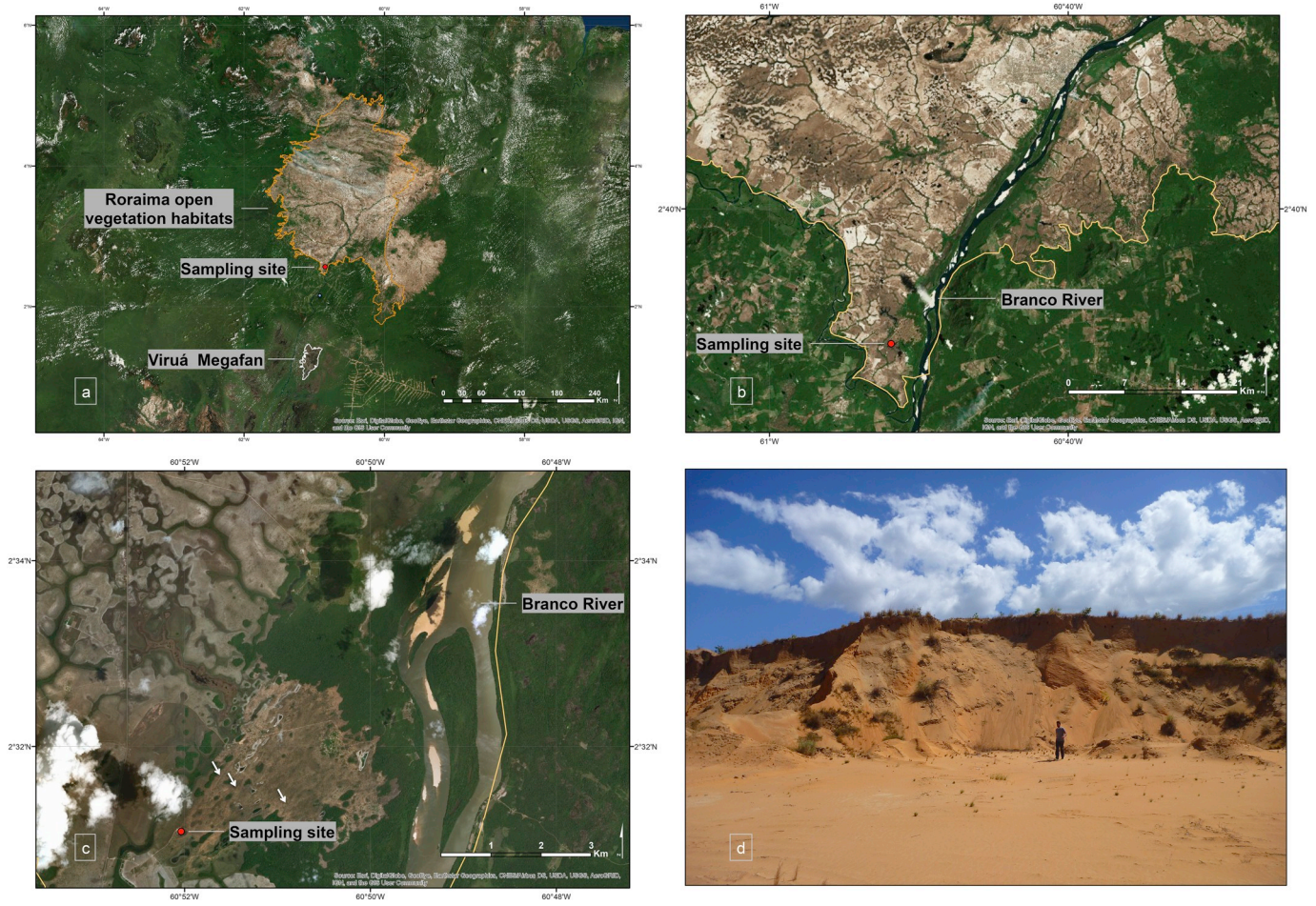

Fig. 2. (a) The orange and white lines border the open vegetation habitats in Roraima State, and Viruá Megafan, respectively, in northern Amazon. (b) Close-up view of the study area showing the drainage configuration and Branco River. (c) Vegetated and unvegetated fluvial sand bars contrast with fully vegetated river banks. Arrows show the position of degraded parabolic dunes that migrate to the SW. (d) The studied sediment profile. Maps by World Image basemap from ArcGIS with attributes displayed in the lower right corner of each map. (For interpretation of the references to color in this figure legend, the reader is referred to the web version of this article.)

S by relic drainage pathways and the E and N by semi-deciduous forests of the Branco River banks. The length and elevation of the vegetation-stabilized arms pointing upwind can reach up to ~0.4 km and 10 m, respectively.

The 8.7-m sediment profile studied herein consists of fluvial silty sand deposits overlain unconformably by eolian sand dunes that are stabilized by savanna vegetation. Spodic Quartzipsamment soils with evidence of lateral podzolization support the vegetation (Mendonça et al., 2014). This study site is located in the Roraima State, northern Brazil (2.518829° N, 60.866381° W; Figs. 1, and 2a, b, c, and d) at an altitude of 80 m and situated 2.5 km west of the Branco River, which enters the Negro River ca. 350 km upstream from the Negro River mouth (Fig. 1). Such location is part of an area of approximately 40,000 km^2 of open vegetation situated on the upper Branco River basin, extending into Guyana (e.g., Alencar et al., 2006; Capurucho et al., 2013; Fig. 1). This area is underlain by the Upper Cenozoic Boa Vista Formation which consists predominantly of sands and sandy clays with intercalated gravel layers (Montalvão et al., 1975), probably deposited in fluvio-lacustrine environments (Sena Costa et al., 1996), or alluvial fans (Riker and Horbe, 2007). The Roraima State open vegetation habitats are bordered to the N, W, and E by elevated areas from the Guyana Shield (predominantly Precambrian igneous and metamorphic rocks) reaching up to 1000 m in altitude (Fig. 1). Low-relief surfaces (40–120 m) and dendritic drainage networks connecting to the southward-flowing Branco River (Fig. 2b and c; Latrubesse and Nelson, 2001) prevail in the study area. These geomorphic features were formed mostly by degraded eolian dunes or alluvial deposits stabilized by open grasslands and scrubby vegetation (Fig. 2c; e.g., Capurucho et al., 2013) like the Viruá Megafan deposit (Fig. 2a). This deposit consists primarily of WSV where mixed sandy substrates originated from various depositional landforms including active or abandoned fluvial channels, overbank sand sheets, terminal fan lobes, and parabolic sand dunes (Rossetti et al., 2012).

1.2. Climate setting

Open vegetation areas in northern Amazonia are exposed to a seasonal antiphased relationship between low-level winds and rainfall related to the landward effects of the position of the Intertropical Convergence Zone (ITCZ; Fig. 1 inset). During boreal winter, ITCZ shifts to the Southern Hemisphere generate NE winds that peak between December and March, reaching speeds of 8 m s^{-1} (INMET, 2016). This wind direction is in agreement with the SW-oriented paleodunes found in the study area (Fig. 2c; Latrubesse and Nelson, 2001). In turn, during boreal summer an ITCZ shift to the Northern Hemisphere moves the tropical rainbelt to the study area and yields up to 1600 mm annual rainfall (INMET, 2016), mainly between April and August. Wind and rain distribution are affected by local orographic configuration (Fig. 1) that enhances wind speeds and limits rainfall through a funneling effect and rain shadow, respectively (Barbosa, 1997).

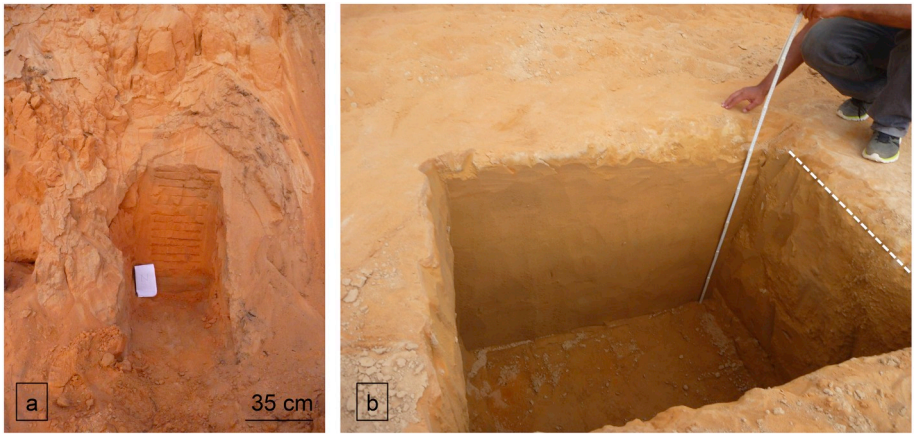

Fig. 3. (a) Section of the eolian sands. (b) Trench excavated to obtain the fluvial deposits (Boa Vista formation). Dashed lines indicate an unconformity between fluvial and the overlain eolian deposit.

2. Methods

2.1. Sampling

To obtain the eolian sand dune and the Boa Vista Formation silty sand samples from the studied profile, the talus slope was removed, and a 1-m deep trench was excavated, respectively (Fig. 3a and b). Samples were taken from fresh surfaces in intervals of 0.5 to 1.0 m for OSL dating (12 samples) and at every 5 cm for sedimentological analysis (170 samples). Charcoal samples were collected for radiocarbon dating (three samples) in the same dune deposit between the surface and 1.6 m depth in a radius of 5 m from the top of the studied section.

2.2. Chronology

Samples collected in aluminum tubes were dated in 2016 by OSL using the single-aliquot regenerative dose protocol applied to quartz (SAR; Murray and Wintle, 2000; Wintle and Murray, 2006) at the Luminescence and Gamma Spectrometry Laboratory (LEGaL) at the University of São Paulo (USP). Samples were prepared in the laboratory under subdued red/amber light according to the methods outlined by Aitken (1998). The 180–250 μm grain size fraction was obtained by wet sieving, followed by chemical treatment with 27% H_2O_2 and 10% HCl to remove organic compounds and carbonates, respectively. Quartz grains (2.65 g cm^{-3}) were isolated from heavy minerals and feldspar grains through gravity settling using lithium metatungstate solutions at densities of 2.75 g cm^{-3} and 2.62 g cm^{-3}, respectively. Subsequently, the quartz concentrates were treated with 48–51% HF for 40 min to remove any remaining feldspar (especially plagioclase) and outer rinds of quartz grains dosed by alpha particles.

Aliquots of ~400 quartz grains were mounted in steel cups for equivalent dose determination. These luminescence measurements were executed in a Risø TL/OSL DA-20 reader equipped with a built-in beta radiation source (^{90}Sr/^{90}Y), delivering a dose rate of 0.119 Gy s^{-1}. This reader contained blue (470 nm) and infrared (870 nm) light-emitting diodes (LED) for stimulation, and a Hoya U-340 filter for light detection in the ultraviolet band. A dose recovery test was executed after bleaching aliquots by sun exposure for 3 h. For this test, beta radiation doses of 0.6, 5.3, and 23.8 Gy were applied to samples ROR-140, ROR-40, and ROR-P-0, respectively, at a pre-heat temperature of 200 °C. The SAR protocol used for equivalent dose estimation is described in Appendix A. The equivalent dose was calculated by exponential fitting of the dose-response data only when recycling ratios were in the 0.9–1.1 range, and recuperation lower than 5%. Feldspar contamination was examined by repeating the first regeneration dose at the end of the SAR sequence and using infrared stimulation at 60 °C before the blue stimulation. Aliquots were rejected when an infrared stimulated luminescence signal was detected, or the OSL signal was significantly depleted following infrared stimulation. The equivalent dose was determined through the central age model (Galbraith et al., 1999) using at least 16 accepted quartz aliquots per sample. To calculate dose rates, the specific activities (Bq kg^{-1}) of ^{238}U, ^{232}Th and ^{40}K radionuclides were appraised through high-resolution gamma-ray spectrometry using an high-purity germanium detector (energy resolution of 2.1 KeV and relative efficiency of 55%) in an ultralow background shield at LEGaL-USP after keeping dry samples (200–300 g) in sealed plastic containers for at least 28 days for radon equilibration. Conversion factors were used for beta and gamma dose rates calculation through radionuclide concentrations (Guérin et al., 2011). The cosmic dose rate was calculated using sample depth, altitude, longitude, and latitude (Prescott and Stephan, 1982). Moisture content was obtained from the water weight relative to dry sample weight after drying the samples in an oven for 48 h at 110 °C. Ages and associated errors for intermediate sediment samples were linearly interpolated from OSL ages.

Charcoal samples were dated by Accelerator Mass Spectrometry (AMS) radiocarbon dating at the Beta Analytic Laboratory (Florida, USA). Results were calibrated using the IntCal13 calibration curve (Reimer et al., 2013) and the Calib 7.1 software (Stuiver et al., 2017).

2.3. Sedimentological analysis

Bulk sedimentological samples collected at the same location as the OSL dating samples were examined with a binocular microscope to estimate mineralogy. Also, they were subjected to heavy mineral analysis in the very fine sand fraction (63–125 μm). For this analysis, samples were separated by gravity settling in bromoform ($CHBr_3$, density of 2.83–2.89 g cm^{-3}) and placed on glass slides using Canada balsam for optical study under the polarizing microscope. Three hundred non-micaceous transparent heavy mineral grains were counted through the ribbon method (Galehouse, 1971). Minerals were represented as a percentage of grains within the heavy mineral assemblage. The zircon-to-rutile ratio (ZRi) was used as a provenance index (Morton and Hallsworth, 1994) through a dedicated count of 300 grains per mineral pair.

All bulk sedimentological samples were analyzed for grain size distribution, reflectance, and magnetic susceptibility measurements. Grain size distribution was obtained using a Malvern Mastersizer 2000 laser diffraction granulometer equipped with a Hydro 2000MU attachment and a built-in ultrasonic device at the Sedimentology Laboratory of Institute of Geosciences at USP. Results were tabulated in 1-phi interval classes and classified according to Wentworth (1922).

Grain size data were presented through descriptive statistics as mean diameter and standard deviation. To acquire reflectance data, samples were made into a slurry with distilled water and subsequently poured on transparent glass slides and let to dry for a day. The dried slides were then analyzed at the Luiz de Queiroz College of Agriculture at USP for: (i) diffuse color reflectance in the visible spectra (400×10^{-9} m to 700×10^{-9} m wavelength) to obtain the a* color parameter using a Minolta CM-700d Spectrophotometer; (ii) reflectance (R) using hyperspectral data contained on contiguous spectral channels (between 400 and 2500 nm wavelength) taken with a FieldSpec Pro spectroradiometer. The (R) value of the samples was transformed into absorbance ($\log_{10}$ R) and analyzed by principal component analysis (PCA) using the Unscrambler 9.7 software as a multivariate analysis technique to correlate wavelength information with sample depth. Measurements of the low-field magnetic susceptibility (MS) were conducted at room temperature using a Kappabridge MFK1-FA (AGICO Ltd) system at the Institute of Astronomy and Geophysics at USP with two excitation frequencies (976 and 15,616 Hz) and an applied field of 200 A m^{-1}. Results were mass-normalized and expressed in $m^3 kg^{-1}$.

3. Results

The eolian dune sediments were composed mostly of poorly-sorted orange fine sand, whereas the Boa Vista Formation fluvial deposit was characterized by extremely poorly-sorted brownish coarse silt (Figs. 3a and b, respectively, and 4a). Both deposits shared a high concentration of quartz (> 98%) and mostly similar heavy mineral assemblages and ZRi (Table 1).

Quartz grains from the studied sediments presented the following favorable characteristics for OSL dating: (i) dose recovery tests with calculated-to-given dose ratios from 0.97 ± 0.01 to 1.07 ± 0.01, comparable to other studies from elsewhere (e.g., Murray and Wintle, 2003); (ii) OSL signals dominated by the fast component (Fig. 5a); (iii) dose-response curves well described by an exponential function (Fig. 5b); and (iv) equivalent dose distributions with overdispersion between 7 and–36% (Fig. 5d, e, and f; Table 2a) except for the topmost sample from the sediment succession profile collected at 0.3 m depth that showed overdispersion of 41%. As a result of using ~400 quartz grains in the cups, the overdispersion of the equivalent dose distribution values was most likely underestimated. This underestimation was demonstrated by analyzing eolian samples from the Netherlands that showed differences of ~ + 6.5% in overdispersion values when analyzing aliquots of 80 instead of 500 grains (Cunningham et al., 2011). Even if we take into account the results obtained by these authors, our samples would still be considered well-bleached sediments (~ < 35% in overdispersion; Arnold and Roberts, 2009) without significant post-depositional mixing resulted from bioturbation. All samples showed relatively low potassium, thorium, and uranium concentration values, which are characteristic of Brazilian sediments from shield areas (Guedes et al., 2013), thus increasing the contribution of cosmic dose rate to the total dose rate (Table 2a). To tackle this situation, dose rates were calculated considering a gradual accumulation of sediments over time (Munyikwa, 2000). Sediment burial ages ranged between 51.7 ± 4.3 ka and 1.1 ± 0.1 ka. The OSL and ^{14}C ages (Table 2a and b) showed a coherent stratigraphic sequence, considering that samples for radiocarbon dating were obtained from slightly different depths in the same dune. Furthermore, the stratigraphic order of the OSL ages suggests an absence of significant contribution of pedo- or bioturbation (e.g., Lomax et al., 2007).

Overlapping OSL ages with associated errors between 23.1 ± 1.3 ka and 17.2 ± 0.9 ka were grouped in a time interval that encompasses 58% of the sand overburden (Figs. 5c and 6a), whereupon an age model was established associating the oldest and youngest age with the bottommost and topmost sample location, respectively. This time interval fits within the onset of the LGM at 23 ka (Mix et al., 2001) down to the duration of Heinrich Stadial 1 from 18.1 until 14.7 ka (Stríkis et al., 2015) and is henceforth called LGM/HS1 (Fig. 5c). The pre-LGM/HS1 sediments (deposited between 51.7 ± 4.3 ka and 27.8 ± 1.7 ka) show relatively stable low values of MS and a* (Fig. 6b and c, respectively). The boundary between the fluvial pre-LGM/HS1 and eolian LGM/HS1 deposits is well represented by a sharp increase of a* and decrease of MS records. The post-LGM/HS1 sands present increasing MS and decreasing a* values over time (Fig. 6b and c, respectively). PCA analysis based on reflectance variables shows separate clusters of data for the pre-LGM/HS1, LGM/HS1, and post-LGM/HS1 periods (Fig. 4b).

Thus, sediments from the study site reveal a succession of three depositional units starting with a basal unit of pre-LGM/HS1 fluvial sediments. These fluvial sediments are overlain by a 5-m thick unit of eolian dune sands deposited under high sediment accumulation rates

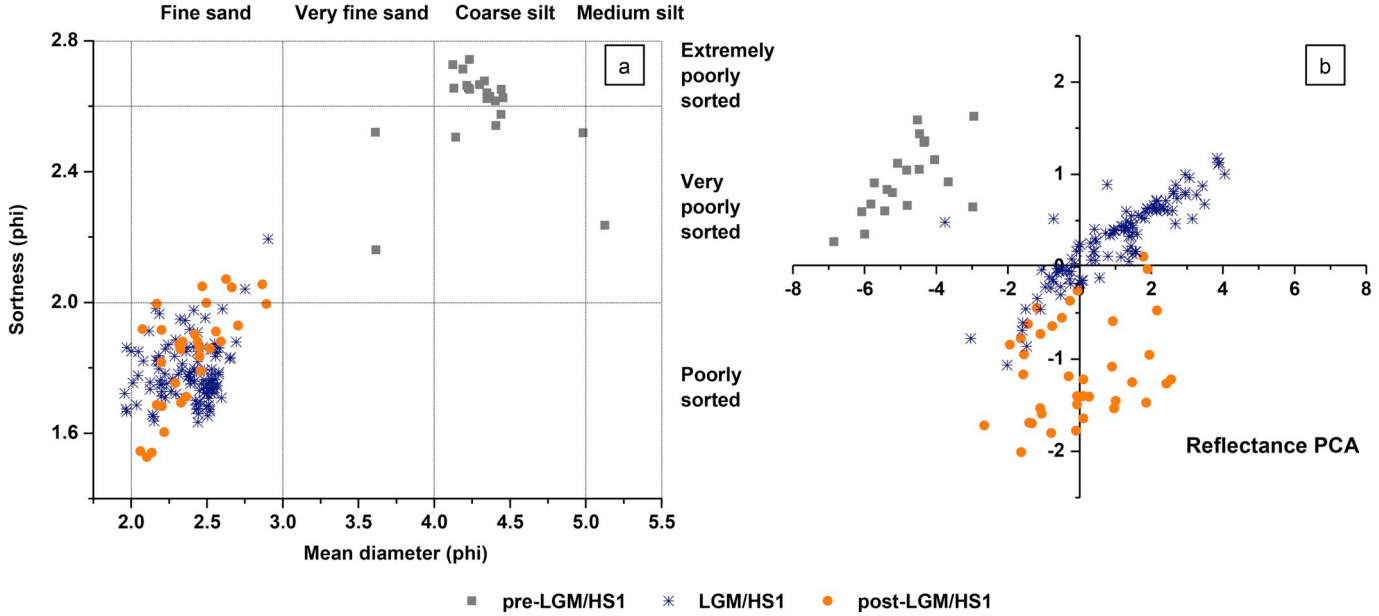

Fig. 4. (a) Grain size distribution statistics showing the textural differences between fluvial pre-LGM/HS1, and eolian LGM/HS1 and post-LGM/HS1 deposits. (b) Principal component analysis reflectance data.

Table 1
Heavy mineral data.

Period	Sample #	Depth (m)	zircon	tourmaline	staurolite	rutile	sillimanite	kyanite	ZRi
post-LGM/HS1	ROR-140	0.30	47%	3%	3%	3%	41%	2%	0.93
	ROR-130	0.80	22%	14%	12%	2%	47%	4%	0.92
	ROR-120	1.30	71%	1%	0%	1%	26%	0%	0.98
	ROR-110	1.80	63%	3%	5%	0%	24%	5%	1.00
LGM/HS1	ROR-080	3.30	48%	1%	1%	0%	46%	4%	1.00
	ROR-060	4.30	30%	12%	9%	2%	38%	8%	0.93
	ROR-040	5.30	74%	5%	19%	0%	0%	3%	1.00
	ROR-020	6.30	10%	15%	6%	2%	63%	4%	0.80
	ROR-001	7.25	78%	4%	8%	0%	0%	10%	1.00
	P-18	7.80	68%	3%	5%	1%	20%	3%	0.99
pre-LGM/HS1	P-10	8.20	43%	2%	4%	0%	48%	2%	0.99
	P-0	8.70	40%	2%	2%	2%	54%	1%	0.96

($0.055\ cm\ yr^{-1}$; Fig. 5c) during the LGM/HS1 time interval. In turn, this unit is overlain by a ~2-m thick unit of eolian sand formed under low sediment accumulation rates ($0.012\ cm\ yr^{-1}$; Fig. 5c) during the post-LGM/HS1 period.

4. Discussion

4.1. The formation of source-bordering dunes in northern Amazonia

The data presented in this paper suggest that before 23.1 ± 1.3 ka (pre-LGM/HS1 period), sediments had already been accumulating in the study area within fluvial systems that dominated the upper Branco River basin in northern Amazonia. This suggestion agrees with OSL ages of fluvial terraces from the lower Branco River obtained by Cremon et al. (2016). Also, our data show no evidence of eolian activity from 51.7 ± 4.3 ka to the onset of the LGM (Fig. 4a), indicating that during the pre-LGM/HS1 period the studied area did not experience climate conditions that prevailed subsequently.

The similar heavy mineral assemblages and ZRi of the fluvial (pre-LGM/HS1 period) and the eolian (LGM/HS1 period) sands indicate a common sediment source (Table 1). Apparently, the dunefield was built from locally reworked fluvial sands that became available through a retraction of perennial fluvial channels under drier conditions. The proximity of these dunes to the Branco River channel indicates limited transport pathways and dune migration. Indeed, the poor sorting of the LGM/HS1 and post-LGM/HS1 eolian sands (Fig. 4a) suggests that these sediments were airborne for short distances. The connection between poorly-sorted eolian sands and limited travel distance has been documented in other studies (e.g., Swezey et al., 2016).

Dunes formed downwind adjacent to a local inland sediment source (lakes or rivers), often as parabolic or linear dunes are usually called supply-limited source-bordering eolian dunes (Hesse, 2014 and references therein; Sankey et al., 2018 and references therein). These dunes remain active as long as sediments are available and strong winds or low humidity constrain vegetation growth. Usually, because of their limited size and spatial arrangements, they indicate localized and pulsed dune activity episodes (Maroulis et al., 2007). Source-bordering dune activity also peaked around the LGM/HS1 in the Colombian and Venezuelan Llanos (Carr et al., 2016; Fig. 1) where lowland savannas overlie eolian sands. Studies of eolian dunes in Amazonia are scarce (Carneiro Filho et al., 2002; Latrubesse and Nelson, 2001; Teeuw and Rhodes, 2004), despite their high paleoclimate relevance. Perhaps, the reason for the small number of studies is that these dunes may often remain predominantly buried under dense vegetation, or their morphology may be degraded, and are thus indistinguishable in remote sensing images or field surveys.

4.2. The correlation between dune building in northern Amazonia and ITCZ shifts during the late Quaternary

4.2.1. The LGM record

Our data show that eolian dune activity in Roraima started around 23 ka, pointing to favorable dune-building conditions already at the onset of the LGM. This framework is consonant with simulations of the

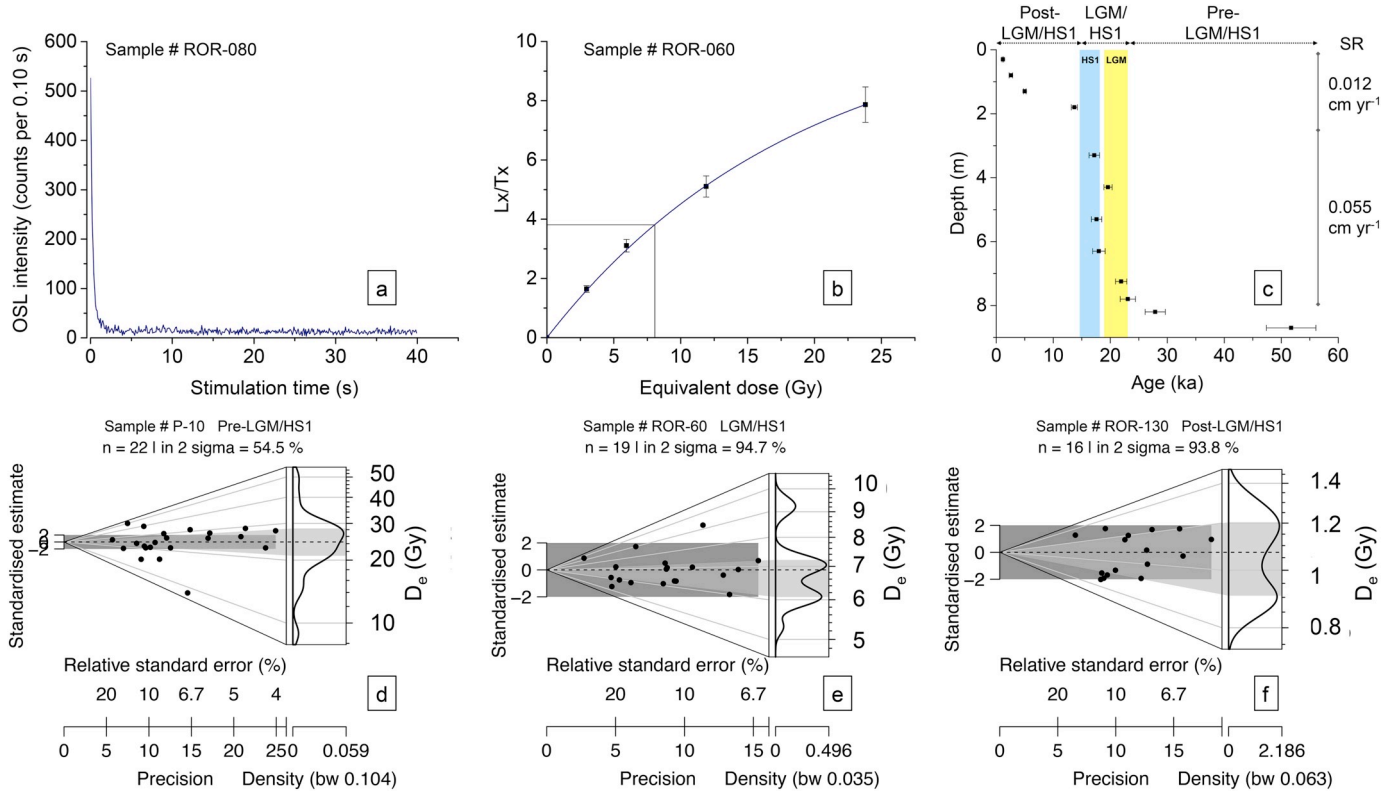

Fig. 5. Luminescence characteristics of quartz aliquots from the studied sediments: (a) OSL decay curve (natural signal); (b) Dose-response curve. (c) Optically stimulated luminescence ages and associated errors plotted against sediment burial depth. SR = Sediment accumulation rate. LGM and HS1 boundaries defined by Mix et al. (2001) and Stríkis et al. (2015), respectively. (d, e, and f) Abanico plots (Dietze et al., 2016) for equivalent dose (D_e) distribution of pre-LGM/HS1, LGM/HS1, and post-LGM/HS1 samples, respectively.

LGM climate that suggest a negative precipitation anomaly over most of Amazonia (Scheff et al., 2017) and agrees with studies showing a predominant position of the ITCZ in the Southern Hemisphere during this period (e.g., Chiang et al., 2003; Chiang and Bitz, 2005). Also, recent analyses have suggested that some areas in Amazonia were drier during the LGM. For example, oxygen isotope records of speleothems from Paraíso Cave in eastern Amazonia (Fig. 1) indicate that the highest $\delta^{18}O$ values during the LGM (Fig. 6e) correspond to a humidity decrease of 58% relative to current humidity (Wang et al., 2017). These measurements are consistent with a plant-wax δD time series obtained from marine sediment core GeoB16224–1 collected off French Guiana (Fig. 1); this proxy is interpreted as a record of changes in precipitation over lowland Amazonia, showing that the LGM was the driest period during the last 50 ka (Häggi et al., 2017). Likewise, a core record from Pata Lake (Fig. 1) suggests the presence of a deciduous forest cover during the LGM that is attributed to a drier climate during this period relative to modern conditions (D'Apolito et al., 2017). It is noteworthy, however, that the LGM negative precipitation anomaly described for northern Amazonia and eastern Amazonia may have had different triggering mechanisms. Resolving each mechanism is beyond the scope of this manuscript.

4.2.2. The HS1 record

Extreme migration of the ITCZ to the Southern Hemisphere during HS1 has been widely documented (e.g., Arz et al., 1998; Deplazes et al., 2013; Mulitza et al., 2017). Recently, an extensive compilation of HS1 paleo-moisture records from tropical South America presented by Zhang et al. (2016) supports the occurrence of a negative precipitation anomaly to the north of the Equator in this region during HS1. Through model experiments, these authors showed both a decrease in precipitation as well as an increase in the strength of the NE trade winds over the study area during HS1. Likewise, a marked decrease in precipitation in the northernmost section of Amazonia during the HS1 is reported by Crivellari et al. (2018). These authors analyzed a marine sediment core off of the Amazon River mouth using isotope, inorganic, and organic geochemistry. The response of eolian dunes to climate is well recorded in NE Brazil (Southern Hemisphere tropics) where persistent southward shifts of the ITCZ provoked increased precipitation benefitting fast stabilization of a 16,000 km^2 coastal dunefield during HS1 (Guedes et al., 2017).

4.2.3. The effects of a drier LGM and HS1 in the study area

The drier conditions during the LGM/HS1 period in northern South America were ideal for the formation of the eolian dunes studied herein by: (i) releasing loose sediments from exposed fluvial sand bars and channels to wind entrainment; and (ii) activating sands from vegetated terrains by the combination of strong winds and dry conditions. Dune-building during the LGM/HS1 period is supported by the lowest MS and highest a* values in our data (Fig. 6b and c, respectively). A high a* parameter indicates a shift from green to red and is usually associated with a higher contribution of authigenic hematite. The presence of hematite even in minimal amounts may contribute disproportionally to the color of sediments (e.g., Deaton and Balsam, 1991). Although the MS signal may be derived primarily from detrital ferromagnetic minerals (e.g., Maher, 1988), the combination of MS and reflectance data indicates that at least part of the signal comes from authigenic mineral varieties. Accordingly, authigenic hematite frequently correlates to drier depositional conditions (e.g., Balsam et al., 2004). Episodic rainfall suggested in this paper by peaks of MS, and a* values would replenish the fluvial sediment stock to be subsequently entrained by the wind during the predominantly dry LGM/HS1 period. Thus, the source-bordering dunes at the study site developed during extended intervals of dryness and persistent strong winds interspersed with intermittent short-lived precipitation events during the LGM/HS1 period.

Table 2
(a) Luminescence data. O.D. = overdispersion in the equivalent dose distribution. Moisture content for all samples was between 3 ± 2% and 9 ± 5%. (b) Radiocarbon ages. Samples for radiocarbon dating were obtained in the same dune but not in the same section used for collecting the OSL samples. Slight variations in altitude (up to ± 0.3 m) must be considered when comparing the depth between the OSL and radiocarbon samples.

	Period	Sample #	Depth (m)	Approved aliquots	Dose (Gy)	O.D.	K (%)	Th (ppm)	U (ppm)	Cosmic dose rate (Gy ka^{-1})	Total dose rate (Gy ka^{-1})	Age (ka)
a	post- LGM/HS1	ROR-140	0.30	19	0.39 ± 0.04	41	0.015	1.003	0.332	0.171 ± 0.008	0.337 ± 0.012	1.1 ± 0.1
		ROR-130	0.80	16	1.04 ± 0.03	9	0.022	1.538	0.440	0.163 ± 0.008	0.403 ± 0.014	2.5 ± 0.3
		ROR-120	1.30	20	2.18 ± 0.04	8	0.028	1.763	0.503	0.161 ± 0.008	0.436 ± 0.016	5.0 ± 0.2
		ROR-110	1.80	20	5.86 ± 0.25	16	0.029	1.674	0.506	0.156 ± 0.007	0.425 ± 0.015	13.6 ± 0.5
	LGM/HS1	ROR-080	3.30	17	6.06 ± 0.23	13	0.016	1.383	0.343	0.143 ± 0.007	0.340 ± 0.017	17.2 ± 0.9
		ROR-060	4.30	19	6.84 ± 0.16	7	0.027	1.614	0.265	0.135 ± 0.006	0.341 ± 0.013	19.6 ± 1.1
		ROR-040	5.30	15	6.49 ± 0.23	9	0.040	1.580	0.336	0.128 ± 0.006	0.359 ± 0.014	17.6 ± 0.7
		ROR-020	6.30	21	6.27 ± 0.21	8	0.037	1.520	0.340	0.121 ± 0.006	0.341 ± 0.012	18.0 ± 0.8
		ROR-001	7.25	20	6.94 ± 0.28	18	0.031	1.297	0.317	0.114 ± 0.005	0.311 ± 0.011	21.9 ± 1.0
		P-18	7.80	19	17.20 ± 0.88	18	0.022	5.460	1.120	0.111 ± 0.005	0.745 ± 0.031	23.1 ± 1.3
	pre-LGM/HS1	P-10	8.20	22	23.79 ± 1.82	33	0.026	7.042	1.235	0.109 ± 0.005	0.851 ± 0.032	27.8 ± 1.7
		P-0	8.70	20	44.52 ± 2.81	28	0.014	7.440	1.310	0.106 ± 0.005	0.858 ± 0.031	51.7 ± 4.3

	Period	Sample #	Depth (m)	Measured age (yrs BP)	$^{13}C/^{12}C$ (VPDB, ‰)	Conventional age (yrs BP)	2Ã calibrated age (yrs BP)
b	post-LGM/HS1	PSG26D	0.40	1150 ± 30	-25.4	1140 ± 30	970-1140
		PSG26E	1.50	4200 ± 40	-25.0	4200 ± 40	4620-4790
		PSG26C	1.60	3770 ± 40	-27.1	3740 ± 40	3980-4230

During the post-LGM/HS1 period, the contribution of sediments from fluvial sources to eolian dune-building decreased because of the seasonally wetter climate as inferred from Cariaco Basin, Paraíso Cave (Fig. 6d and e, respectively), and Pata Lake records. With an increasingly wetter climate, vegetation density probably expanded in the vicinity of river channels and fluvial sand bars. Denser vegetation is more resistant to wind activity and helps to trap eolian sands transported from areas such as unvegetated fluvial sand bars, thus limiting sediment availability for dune-building (e.g., Loope and Swinehart, 2000). Reduced sediment availability may also be related to the expansion of muddy substrates in fluvial bar tops and floodplains, where the wetter climate after HS1 favored shifts from an eolian-alluvial fan (sandy plain) to a tributary fluvial (muddy floodplain) depositional system. Thus, during the post-LGM/HS1 period, eolian dune building was no longer rejuvenated by newly deposited sands from fluvial sources, and eolian sediment accumulation rates dropped almost five-fold (Fig. 5c). Instead, sands for eolian dune-building would be provided during episodical drier and windier events that could remobilize sediments from exposed fluvial sand bars or previously stabilized dunes. Unevenly-distributed peaks of increasing MS and decreasing a* reflect these conditions. Also, discrete signatures shown in the reflectance PCA between the LGM/HS1 and post-LGM/HS1 periods (Fig. 5b) suggest intensification of pedogenic processes and increasing soil moisture after HS1.

The dune-building paleoenvironmental archive presented in this study is consistent with data from the Cariaco Basin (e.g., Deplazes et al., 2013; Fig. 6d) that shows no other high-magnitude abrupt climate event after HS1 that could foster prolonged dry and windy conditions to mobilize riverine sediments by eolian processes. Accordingly, our record agrees with other proxy data that emphasize the marked strength of HS1 in the Northern Hemisphere tropics (e.g., McGee et al., 2014; Portilho-Ramos et al., 2017).

4.3. The connection between abrupt climate changes and biota adapted to open vegetation environments

Sandy substrates in Amazonia are not exclusively derived from eolian activity. They were also formed by sediment accumulation in distributary alluvial systems during drier phases (Rossetti et al., 2012; Rossetti, 2014). Thus, drier conditions favored the combined activation and expansion of eolian and alluvial depositional systems, which led to the spreading of open vegetation habitats embedded within the forest matrix. There is growing biogeographic evidence to support the expansion of sandy substrates during the LGM and HS1 reported in this paper. Notably, population growth of some bird species in Roraima State is linked to the open vegetation habitats formed during the dry and windy LGM/HS1 period, and the subsequent wetter post-LGM/HS1. Despite the lack of demographic data related to species from savanna enclaves, molecular signals of population expansion have been increasingly reported for bird specialized in WSV (Capurucho et al., 2013, 2018; Matos et al., 2016; Ferreira et al., 2018). For example, phylogeographic studies using sequencing DNA of the WSV-specialist bird

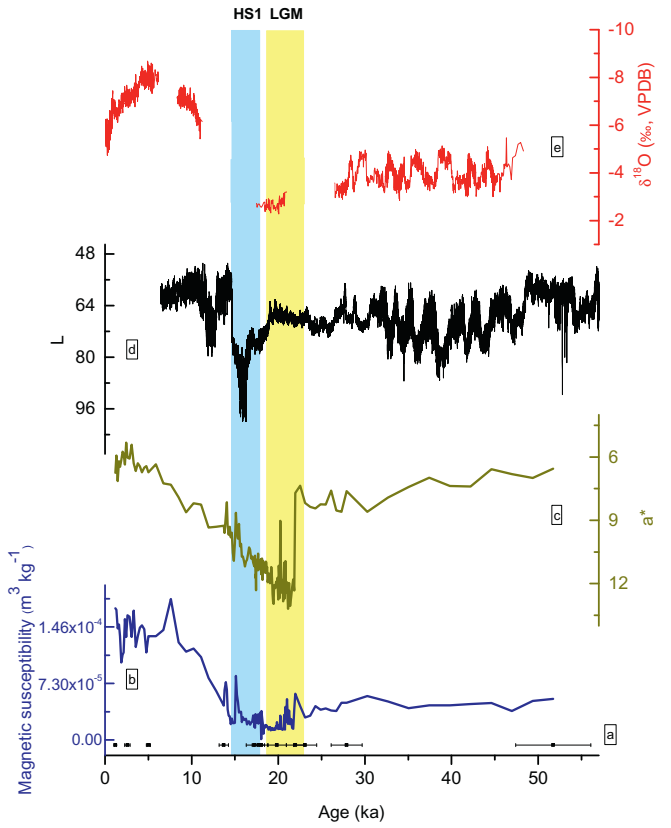

Fig. 6. (a) OSL ages. (b and c) magnetic susceptibility and a* reflectance parameter, respectively. (d) The Cariaco Basin paleoclimate proxy L that correlates with southward migrations of the ITCZ in northern South America (Deplazes et al., 2013). (e) Paraíso Cave speleothem records show the lowest $\delta^{18}O$ values during the LGM. Data from this speleothem are missing for three short gaps (Wang et al., 2017).

Xenopipo atronitens suggest that its demographic expansion in the WSV of Roraima State started around the LGM (Capurucho et al., 2013). Likewise, analyses of sequences of one mithocondrial and one nuclear gene region of the WSV-restricted birds *Achyphonus phoenicius* and *Polytmus theresie* suggest that their population expansion is linked to the development of new or expanding white sand environments during the LGM (Matos et al., 2016). The onset of a drier climate in northern Amazonia during the LGM reported here also agrees with a recent study by Nazareno et al. (2017) that detected significant genetic isolation of an Amazonian shrub across the Negro River, though no genetic differentiation was found across the Branco River. These authors suggest that rather than acting as a barrier to gene flow, a reduced Branco River channel coeval with eolian dune activity during the LGM/HS1 period would have been more permeable to gene flow.

By finding consistency of biotic and abiotic results on open vegetation formation, we believe that our data may contribute to constraining hypotheses about the genomic evolution of species that have not been scrutinized so far. More than 100 plant species are considered endemic to open vegetation habitats (Fine et al., 2010), and of the 195 bird species regularly recorded in WSV, 28 and seven species are considered near-restricted and restricted to these environments, respectively (Borges et al., 2016).

5. Conclusions

This study shows that abrupt climate changes have modulated the distribution of open vegetation environments in northern Amazonia since the Last Glacial Maximum. By presenting the chronology and mechanism for the construction of the eolian sand dunes overlying fluvial substrates, we constrain the timing of formation and evolution of an enclave of open vegetation in northern Amazonia. The association of OSL and radiocarbon chronology with paleoclimate proxies applied to an 8.7-m thick sediment profile indicates that a decrease in precipitation and a strengthening in the NE trade winds occurred during the LGM and HS1. These climate conditions ultimately promoted the formation of sandy substrates that underpinned the expansion of open vegetation in northern Amazonia. These areas were mainly formed alongside river channels when eolian activity was synchronous with persistent shifts of the ITCZ to the Southern Hemisphere. An increase in precipitation and a decrease in NE trade wind strength hindered eolian dune building after HS1. Although the paleoenvironmental framework proposed in this paper is based on data from a single sediment profile, the close-coupling proxy records from this study site and regional paleoclimate data from Cariaco Basin, Pata Lake, Paraíso Cave, and the continental margin off French Guiana suggest that the paleoenvironmental archive presented herein is consistent with regional abrupt climate changes. Importantly, our findings are in agreement with recent reports showing the expansion of biota specialized in open vegetation habitats in northern Amazonia during and after the LGM.

Acknowledgments

We thank Diego Fróes e Souza for his field work assistance. Elaine Sinfroni and Jordana Zampelli were helpful in the sedimentological analysis. We appreciate the funding for field and laboratory work provided by FAPESP (grants 2011/06609-1, 2012/17517-3, 2012/50260-6, and 2016/02656-9), CAPES (Proex 558/2011, grants 1976/2014 and 564/2015), and CNPq (grants 302607/2016-1 and 422255/2016-5). The authors are grateful to the editor and the two anonymous reviewers for their helpful comments and suggestions that improved the quality of this manuscript.

Appendix A. Supplementary data

Supplementary data to this article can be found online at https://doi.org/10.1016/j.gloplacha.2018.09.006.

References

Adeney, J.M., Christensen, N.L., Vicentini, A., Cohn-Haft, M., 2016. White-sand ecosystems in Amazonia. Biotropica 48, 7–23.
Aitken, M.J., 1998. An Introduction to Optical Dating. Oxford University Press, New York.
Alencar, M.M.F., Carneiro, Filho A., Costa, J.A.L., 2006. Mapeamento e dinâmica pré-atual das savanas amazônicas. In: Anais da XV Jornada de Iniciação Científica PIBIC/CNPq/FAPEAM/INPA, Manaus, pp. 93–94.
Anderson, A.B., 1981. White-sand vegetation of Brazilian Amazonia. Biotropica 13, 199–210.
Arnold, L.J., Roberts, R.G., 2009. Stochastic modelling of multi-grain equivalent dose (De) distributions: implications for OSL dating of sediment mixtures. Quat. Geochronol. 4, 204–230.
Arz, H.W., Patzold, J., Wefer, G., 1998. Correlated millennial-scale changes in surface hydrography and terrigenous sediment yield inferred from last-glacial marine deposits off northeastern Brazil. Quat. Res. 50, 157–166.
Balsam, W., Ji, J., Chen, J., 2004. Climatic interpretation of the Luochuan and Lingtai loess sections, China, based on changing iron oxide mineralogy and magnetic susceptibility. Earth Planet. Sci. Lett. 223, 335–348.
Barbosa, R.I., 1997. Distribuição das chuvas em Roraima. In: Barbosa, R.I., Ferreira, E.J.G., Castellon, E.G. (Eds.), Homem, Ambiente e Ecologia em Roraima. Manaus, Brazil, pp. 325–335.
Borges, S.H., Corneluus, C., Ribas, C., Almeida, R., Guilherme, E., Aleixo, A., Moreira, M., 2016. What is the avifauna of Amazonian white-sand vegetation? Bird Conserv. Int. 26, 192–204.
Capurucho, J.M.G., Cornelius, C., Borges, S.H., Cohn-Haft, M., Aleixo, A., Metzger, J.P., et al., Ribas, C.C., 2013. Combining phylogeography and landscape genetics of Xenopipo atronitens (Aves: Pipridae), a white sand campina specialist, to understand Pleistocene landscape evolution in Amazonia. Biol. J. Linn. Soc. 110, 60–76.
Capurucho, J.M.G., Ashley, M.V., Ribas, C.C., Bates, J.M., 2018. Connecting Amazonian, Cerrado, and Atlantic Forest histories: Paraphyly, old divergences, and modern population dynamics in tyrant-manakins (*Neopelma/Tyranneutes*, Aves: Pipridae). Mol. Phylogenet. Evol. 127, 696–705.
Carneiro Filho, A., Schwartz, D., Tatumi, S.H., Rosique, T., 2002. Amazonian paleodunes provide evidence for drier climate phases during the Late Pleistocene–Holocene.

Quat. Res. 58, 205–209.
Carr, A.S., Armitage, S.J., Berrío, J.C., Bilbao, B.A., Boom, A., 2016. An optical luminescence chronology for late Pleistocene aeolian activity in the Colombian and Venezuelan Llanos. Quat. Res. 85, 299–312.
Carvalho, T.M., Carvalho, C.M., 2012. Interrelation of geomorphology and fauna of Lavrado region in Roraima, Brazil-suggestions for future studies. Quat. Sci. J. 61, 146–155.
Chiang, J.C., Bitz, C.M., 2005. Influence of high latitude ice cover on the marine Intertropical Convergence Zone. Clim. Dyn. 25, 477–496.
Chiang, J.C., Biasutti, M., Battisti, D.S., 2003. Sensitivity of the Atlantic intertropical convergence zone to last glacial maximum boundary conditions. Paleoceanography 18, 1–16.
Colinvaux, P., 1987. Amazon diversity in light of the paleoecological record. Quat. Sci. Rev. 6, 93–114.
Cremon, É.H., Rossetti, D.F., Sawakuchi, A.O., Cohen, M.C.L., 2016. The role of tectonics and climate in the late Quaternary evolution of a northern Amazonian River. Geomorphology 271, 22–39.
Crivellari, S., Chiessi, C.M., Kuhnert, H., Häggi, C., da, Costa, Portilho-Ramos, R., Zeng, J.-Y., Zhang, Y., Schefuß, E., Mollenhauer, G., Hefter, J., Alexandre, F., Sampaio, G., Mulitza, S., 2018. Increased Amazon freshwater discharge during late Heinrich Stadial 1. Quat. Sci. Rev. 181, 144–155.
Cunningham, A.C., Wallinga, J., Minderhoud, P.S., 2011. Expectations of scatter in equivalent-dose distributions when using multi-grain aliquots for OSL dating. Geochronometria 38, 424.
D'Apolito, C., Absy, M.L., Latrubesse, E.M., 2017. The movement of pre-adapted cool taxa in north-central Amazonia during the last glacial. Quat. Sci. Rev. 169, 1–12.
Deaton, B.C., Balsam, W.L., 1991. Visible spectroscopy — a rapid method for determining hematite and goethite concentration in geological materials. J. Sediment. Petrol. 61, 628–632.
Deplazes, G., Lückge, A., Peterson, L.C., Timmermann, A., Hamann, Y., Hughen, K.A., Rohl, U., Laj, C., Cane, M.A., Sigman, D.M., Haug, G.H., 2013. Links between tropical rainfall and North Atlantic climate during the last glacial period. Nat. Geosci. 6, 213–217.
Dietze, M., Kreutzer, S., Burow, C., Fuchs, M.C., Fischer, M., Schmidt, C., 2016. The abanico plot: visualising chronometric data with individual standard errors. Quat. Geochronol. 31, 12–18.
Ferreira, M., Fernandes, A.M., Aleixo, A., Antonelli, A., Olsson, U., Bates, J.M., et al., Ribas, C.C., 2018. Evidence for mtDNA capture in the jacamar *Galbula leucogastra/chalcothorax* species-complex and insights on the evolution of white-sand ecosystems in the Amazon basin. Mol. Phylogenet. Evol. 129, 149–157.
Fine, P.V.A., Baraloto, C., 2016. Habitat endemism in white-sand forests: insights into the mechanisms of lineage diversification and community assembly of the Neotropical flora. Biotropica 48, 24–33.
Fine, P.V.A., García-Villacorta, R., Pitman, N.C.A., Mesones, I., Kembel, S.W., 2010. A floristic study of the white-sand forests of Peru. Ann. Mo. Bot. Gard. 97, 283–305.
Galbraith, R.F., Roberts, R.G., Laslett, G.M., Yoshida, H., Olley, J.M., 1999. Optical dating of single and multiple grains of quartz from jinmium rock shelter, northern Australia, part 1, experimental design and statistical models. Archaeometry 41, 339–364.
Galehouse, J.S., 1971. Point Counting. In: Carver, R.E. (Ed.), Procedures in Sedimentary Petrology. Wiley, New York, pp. 385–407.
Guedes, C.C.F., Sawakuchi, A.O., Giannini, P.C.F., Dewitt, R., Aguiar, V.A.P., 2013. Luminescence characteristics of quartz from Brazilian sediments and constraints for OSL dating. An. Acad. Bras. Cienc. 85, 1303–1316.
Guedes, C.C.F., Giannini, P.C.F., Sawakuchi, A.O., Dewitt, R., Aguiar, V.A.P., 2017. Weakening of northeast trade winds during the Heinrich stadial 1 event recorded by dune field stabilization in tropical Brazil. Quat. Res. 88, 369–381.
Guérin, G., Mercier, N., Adamiec, G., 2011. Dose-rate conversion factors: update. Ancient TL 29, 5–8.
Häggi, C., Chiessi, C.M., Merkel, U., Mulitza, S., Prange, M., Schulz, M., Schefuß, E., 2017. Response of the Amazon rainforest to late Pleistocene climate variability. Earth Planet. Sci. Lett. 479, 50–59.
Hesse, P.P., 2014. How do longitudinal dunes respond to climate forcing? Insights from 25 years of luminescence dating of the Australian desert dunefields. Quat. Int. 410, 11–29.
Honorio Coronado, E.N., Dexter, K.G., Pennington, R.T., Chave, J., Lewis, S.L., Alexiades, M.N., et al., Arets, E.J., 2015. Phylogenetic diversity of Amazonian tree communities. Divers. Distrib. 21, 1295–1307.
INMET, 2016. Brazilian Institute of Meteorology. www.inmet.gov.br (Accessed 10 November 2017).
Latrubesse, E.M., Nelson, B.W., 2001. Evidence for late Quaternary aeolian activity in the Roraima–Guyana region. Catena 43, 63–80.
Lomax, J., Hilgers, A., Twidale, C.R., Bourne, J.A., Radtke, U., 2007. Treatment of broad palaeodose distributions in OSL dating of dune sands from the western Murray Basin, South Australia. Quat. Geochronol. 2, 51–56.
Loope, D.B., Swinehart, J.B., 2000. Thinking like a dune field: geologic history in the Nebraska Sand Hills. Great Plains Res. 10, 5–35.
Maher, B.A., 1988. Magnetic properties of some synthetic sub-micron magnetites. Geophys. J. Int. 94, 83–96.
Maroulis, J.C., Nanson, G.C., Price, D.M., Pietsch, T., 2007. Aeolian–fluvial interaction and climate change: source-bordering dune development over the past ~ 100ka on Cooper Creek, central Australia. Quat. Sci. Rev. 26, 386–404.
Matos, M.V., Borges, S.H., d'Horta, F.M., Cornelius, C., Latrubesse, E., Cohn-Haft, M., Ribas, C.C., 2016. Comparative phylogeography of two bird species, Tachyphonus phoenicius (Thraupidae) and Polytmus theresiae (Trochilidae), specialized in Amazonian white-sand vegetation. Biotropica 48, 110–120.
McGee, D., Donohoe, A., Marshall, J., Ferreira, D., 2014. Changes in ITCZ location and cross-equatorial heat transport at the Last Glacial Maximum, Heinrich Stadial 1, and the mid-Holocene. Earth Planet. Sci. Lett. 390, 69–79.
Mendonça, B.A.F., Simas, F.N.B., Schaefer, C.E.G.R., Fernandes Filho, E.I., do Vale Júnior, J.F., de Mendonça, J.G.F., 2014. Podzolized soils and paleoenvironmental implications of white-sand vegetation (Campinarana) in the Viruá National Park, Brazil. Geoderma Regional 2, 9–20.
Mittermeier, J.C., Zyskowski, K., Stowe, E.S., Lai, J.E., 2010. Avifauna of the Sipaliwini savanna (Suriname) with insights into its biogeographic affinities. Bull. Peabody Museum Nat. Hist. 51, 97–122.
Mix, A.C., Bard, E., Schneider, R., 2001. Environmental processes of the ice age: land, oceans, glaciers (EPILOG). Quat. Sci. Rev. 20, 627–657.
Montalvão, R.M.G., Muniz, M.B., Issler, R.S., Dalll'agnol, R., Lima, M.I.C., Fernandes, P.E.C.A., Silva, G.G., 1975. Geologia do Território Federal de Roraima. DNPM, Conferência Geológica Interguianas, Anais, 10, Belém, pp. 198–217.
Morton, A.C., Hallsworth, C.R., 1994. Identifying provenance-specific features of detrital heavy mineral assemblages in sandstones. Sediment. Geol. 90, 241–256.
Mulitza, S., Chiessi, C.M., Schefuß, E., Lippold, J., Wichmann, D., Antz, B., et al., Werner, M., 2017. Synchronous and proportional deglacial changes in Atlantic meridional overturning and northeast Brazilian precipitation. Paleoceanography 32, 622–633.
Munyikwa, K., 2000. Cosmic ray contribution to environmental dose rates with varying overburden thickness. Ancient TL 18, 27–34.
Murray, A.S., Wintle, A.G., 2000. Luminescence dating of quartz using an improved single-aliquot regenerative-dose protocol. Radiat. Meas. 32, 57–73.
Murray, A.S., Wintle, A.G., 2003. The single aliquot regenerative dose protocol: potential for improvements in reliability. Radiat. Meas. 37, 377–381.
Nazareno, A.G., Dick, C.W., Lohmann, L.G., 2017. Wide but not impermeable: testing the riverine barrier hypothesis for an Amazonian plant species. Mol. Ecol. 26, 3636–3648.
Portilho-Ramos, R.C., Chiessi, C.M., Zhang, Y., Mulitza, S., Kucera, M., Siccha, M., et al., Paul, A., 2017. Coupling of equatorial Atlantic surface stratification to glacial shifts in the tropical rainbelt. Sci. Rep. 7.
Prescott, J.R., Stephan, L.G., 1982. The contribution of cosmic radiation to the environmental dose for thermoluminescence dating. In: Proceedings of the Second Specialist Seminar on Thermoluminescence Dating, 6. Council of Europe, Strasbourg, pp. 17–25.
Quesada, C.A., Lloyd, J., Schwarz, M., Patino, S., Baker, T.R., Czimczik, C., et al., Santos, A.J.B., 2010. Variations in chemical and physical properties of Amazon forest soils in relation to their genesis. Biogeosciences 7, 1515–1541.
Quesada, C.A., Phillips, O.L., Schwarz, M., Czimczik, C.I., Baker, T.R., Patiño, S., et al., Alvarez Dávila, E., 2012. Basin-wide variations in Amazon forest structure and function are mediated by both soils and climate. Biogeosciences 9, 2203–2246.
Reimer, P.J., Bard, E., Bayliss, A., Beck, J.W., Blackwell, P.G., Ramsey, C.B., et al., Grootes, P.M., 2013. IntCal13 and Marine13 radiocarbon age calibration curves 0–50,000 years cal BP. Radiocarbon 55, 1869–1887.
Riker, S.R., Horbe, A.M.C., 2007. Sedimentos holocênicos da região de Boa Vista (Roraima) para indústria de cerâmica vermelha. In: Rosa-Costa, L.T., Klein, E.L., Viglio, E.P. (Eds.), Contribuições a geologia da Amazonia. Vol. 5. Sociedade Brasileira de Geociências, Belém, pp. 101–112.
Rossetti, D.F., 2014. The role of tectonics in the late Quaternary evolution of Brazil's Amazonian landscape. Earth Sci. Rev. 139, 362–389.
Rossetti, D.F., Zani, H., Cohen, M.C.L., Cremon, É.H., 2012. A Late Pleistocene–Holocene wetland megafan in the Brazilian Amazonia. Sediment. Geol. 282, 276–293.
Sankey, J.B., Kasprak, A., Caster, J., East, A.E., Fairley, H.C., 2018. The response of source-bordering aeolian dunefields to sediment-supply changes 1: effects of wind variability and river-valley morphodynamics. Aeolian Res. 32, 228–245.
Scheff, J., Seager, R., Liu, H., Coats, S., 2017. Are glacials dry? Consequences for paleoclimatology and for greenhouse warming. J. Clim. 30, 6593–6609.
Sena Costa, J.B., Bemerguy, R.L., Hasui, Y., Borges, M.S., Ferreira Júnior, C.R.P., Bezerra, P.E.L., Costa, M.L., Fernandes, J.M.G., 1996. Neotectônica da região Amazônica: aspectos tectônicos, geomorfológicos e deposicionais. GEONOMOS 4, 23–44.
Stríkis, N.M., Chiessi, C.M., Cruz, F.W., Vuille, M., Cheng, H., Souza Barreto, E.A., Bernal, J.P., 2015. Timing and structure of Mega-SACZ events during Heinrich Stadial 1. Geophys. Res. Lett. 42, 5477–5484.
Stuiver, M., Reimer, P.J., Reimer, R.W., 2017. CALIB 7.1 [WWW program]. at. http://calib.org (Accessed 25 March 2017).
Swezey, C.S., Fitzwater, B.A., Whittecar, G.R., Mahan, S.A., Garrity, C.P., González, W.B.A., Dobbs, K.M., 2016. The Carolina Sandhills: quaternary eolian sand sheets and dunes along the updip margin of the Atlantic Coastal Plain province, southeastern United States. Quat. Res. 86, 271–286.
Teeuw, R.M., Rhodes, E.J., 2004. Aeolian activity in northern Amazonia: optical dating of Late Pleistocene and Holocene palaeodunes. J. Quat. Sci. 19, 49–54.
Wang, X., Edwards, R.L., Auler, A.S., Cheng, H., Kong, X., Wang, Y., ... Chiang, H.W., 2017. Hydroclimate changes across the Amazon lowlands over the past 45,000 years. Nature 541, 204–207.
Wentworth, C.K., 1922. A scale of grade and class terms for clastic sediments. J. Geol. 377–392.
Wintle, A.G., Murray, A.S., 2006. A review of quartz optically stimulated luminescence characteristics and their relevance in single-aliquot regeneration dating protocols. Radiat. Meas. 41, 369–391.
Zhang, Y., Zhang, X., Chiessi, C.M., Mulitza, S., Zhang, X., Lohmann, G., ... Wefer, G., 2016. Equatorial Pacific forcing of western Amazonian precipitation during Heinrich Stadial 1. Sci. Rep. 6, 35866.